Assessment on Ground Control Points in Unmanned Aerial System Image Processing for Slope Mapping Studies

Khairul Nizam Tahar[*1], Anuar Ahmad[2], Wan Abdul Aziz Wan Mohd Akib[2], Wan Mohd Naim Wan Mohd[1]

Abstract— The first objective of this study is to investigate the use of light weight rotary-wing UAV for mapping simulation model. The second objective is to determine the accuracy of the photogrammetric output produced from this study. In this study, the photogrammetric output such as stereomodel in three dimensional (3D), contour lines, digital elevation model (DEM) and orthophoto were produced from a simulation model with a dimension of 3m x 1m. In the simulation model, ground control points (GCP) and checked point (CP) were established using a total station. The GCP is used to produce photogrammetric output while the CP is used for accuracy assessment. A Nikon Coolpix consumer digital camera was used in image acquisition of the simulation model. Two methods of image capturing were used. In the first method, the camera was mounted vertically on a rotary-wing UAV and the images were captured at an altitude of 1.2 meters. In the second method, the camera was mounted vertically on a wooden structure at a fixed height (in this case 1.2 meters). After obtaining all the required images, they were then processed using digital photogrammetric software to produce photogrammetric output. Based on the results of this study, it was found that the final product of the rotary-wing UAV was not significantly different from the results acquired from the fixed height data acquisition method. The results of this study also showed that the differences of DEM and digital orthophoto between both methods were relatively small. Finally, it can be concluded that the UAV system can be used for small-scale mapping and other diversified applications, especially for small areas, which involves a limited budget and time constraints.

Index Terms— UAV, Photogrammetry, Stereomodel, DEM, Digital Orthophoto

1 INTRODUCTION

IN 1980, a model of the rotary wing UAV was introduced to be utilized for photogrammetry work. The UAV was able to carry payloads up to 3 kg and had flying range of around 10 to 100 meters. A Rolleiflex camera unit was attached to the bottom of the UAV by installing a camera mount. A professional operator was used to control for hovering operations, landing and flying the unmanned model helicopter [5]. The technology of UAV has experienced various developments over the years. According to [5], there were hundreds of UAV operated by military and civil based organizations for numerous applications. Demand of aerial photogrammetry has increased especially after the development of design, research and production of UAV platform [2], [3]. Numerous UAV's have been developed by organization or individual worldwide including a complete set of UAV which uses high quality fibers as the material for model planes [8]. UAV technology has been utilized in many applications such as farming, surveillance, road maintenance, recording and documentation of cultural heritage [1], [6]. Compared to other mobile systems, the UAV is the most practical solution for low budget projects with time constraints and it requires less manpower [7], [14]. Three dimensional model can be generated using UAV images after going through certain processes. The scale of aerial photographs taken using UAV devices relies on flying height and focal length of digital camera as with most aerial based photographs [13], [14].

In this study, two main hardware were used which include the light weight rotary-wing UAV and high resolution digital camera. Low altitude UAV was the preferred device for data capture because it focuses on large scale mapping which involves small areas only. UAV's are potentially the most suitable equipment that can be used for this sort of project which involves very low cost budget for capturing aerial photograph of small areas. Apart from that, amateur digital camera with high resolution images was attached at the UAV. The amateur digital camera provides small sized images, which will not consume a lot of memory space. Amateur digital cameras have many different selections of resolutions which can be set on the device in which each of them will portray different pixel sizes. Figure 1 shows an example of a UAV (Hexacopter) and amateur digital camera.

(a)

• *Khairul Nizam Tahar is currently pursuing PhD in Geoinformatics in Universiti Teknologi Malaysia, Malaysia. E-mail: nizamtahar@gmail.com*

(b)

Fig. 1. (a) Hexacopter ; (b) Digital Camera

In this study, Nikon Coolpix L4 was used in acquiring simulation model images. Nikon Coolpix digital camera has 3x optical zoom lens and a 2.0" LCD screen. In this study, Micro UAV also known as Hexacopter (Figure 1), was used in acquiring images for the stated model. Hexacopter has 6 blades in which 3 blades rotate in a clockwise direction and the other 3 blades rotate in a counterclockwise direction. The Nikon Coolpix camera was attached at the bottom of Hexacopter to capture aerial images during flight operation. The specification of the rotary wing used in this study is shown in Table 1.

TABLE 1
HEXACOPTER SPECIFICATION (RCHELI,2008)

	Specification
Weight	1.2kg
Rotor	6 rotor
Endurance	Up to 36 minutes
Payload	1kg
GPS on board	Yes
Special function	Automatically return to home location (1st point)
Stabilizer	In-built stabilizer to deal with wind correction
Capture data	Using software to reached waypoints
Flight control	Manual and autonomous
Camera stand	Flexible camera holder

2 RELATED WORK

Helicopter UAV has been investigated in depth for data acquisition as studied [4], [12]. The combination of GPS/INS and helicopter UAV increased the sensitivity of UAV to determine point of measurement on the ground as mentioned by [2], [11], [4], [13]. Many studies have been done to improve the accuracy of GPS on board for reduction of the number of ground control needed during UAV image processing [2]. Remote control helicopters are not designed for large areas but it can be used for small areas such as areas in vicinities of complex buildings which is difficult to be captured by aircrafts of higher speed and altitude. In addition, UAV's cost much cheaper as compared to other aircrafts or terrestrial equipment as mentioned [3], [11], [15]. The uses of Micro UAV's have big potential in forest and agricultural application as studied by Grenzdoffer et al. (2008). It is because UAV's are more flexible and able to obtain data in any weather condition [10]. The special requirement for photogrammetry and GIS (Geographical Information System) process has been studied for various applications such as exterior orientation precision value, systematic aerial survey and metric camera. There are two types of micro UAV's that has been introduced by [5] named as Carolo P330 and SUSI. Low cost micro UAV SUSI powered by 4.2kW two stroke engines, can be controlled manually by the operator from the ground. The accuracy of GCP and x and y image coordinate improves when the percentage of end lap and side lap fulfill the standard block configuration. The accuracy of GCP for Z coordinate is less accurate than the GCP for X and Y coordinates due to the systematic error in focal length with various zoom lenses [9]. The advantages of UAV are in low cost, flexible manoeuvrings, high resolution images, flying under clouds, easy launch and landing and very safe to use [15]. The disadvantages of UAV include payload limitation, small coverage for each image, increasing number of image that need to be processed and large geometric distortion.

3 METHODOLOGY

In this study, the methodology are divided into several phases namely data preparation, data collection, data processing, result, analysis and discussion. Figure 2 depicts flowchart of the research methodology which concentrates on fixed platform and mobile platform. Fixed platform was built from a wooden structure that was not adjustable and it was fixed at 1.2 meter from simulated model while mobile platform using rotary wing UAV flew at altitude 1.2 meter from the simulated model. Both platforms were used to obtain aerial images of simulated model.

The dimension of the simulated model was approximately 3 x 1 metres and was prepared using sand and cement. The simulated model represents a slope area along a road side which has different gradients and slope length. The GCPs were distributed on the simulated model evenly and were established using total station. Camera calibration was carried out to obtain all camera parameters as input for image processing. In the digital image, one of the main important values that should be considered is pixel size. Pixel size will determine the ground coverage area or size of the objects. The size of pixel involves a few elements such as number of pixel for object image, length of an object in real measurement, focal length of camera and flying height during image capturing. Furthermore, each digital camera has different pixel size and it must be calculated in the flight planning phase prior to deploying the UAV. The ground coverage area of one image can be defined by multiplying the scale of the photograph with the resolution of the digital image. The calculation of overlap percentage involves certain parameters such as image resolution, scale, flying height and focal length of the digital camera.

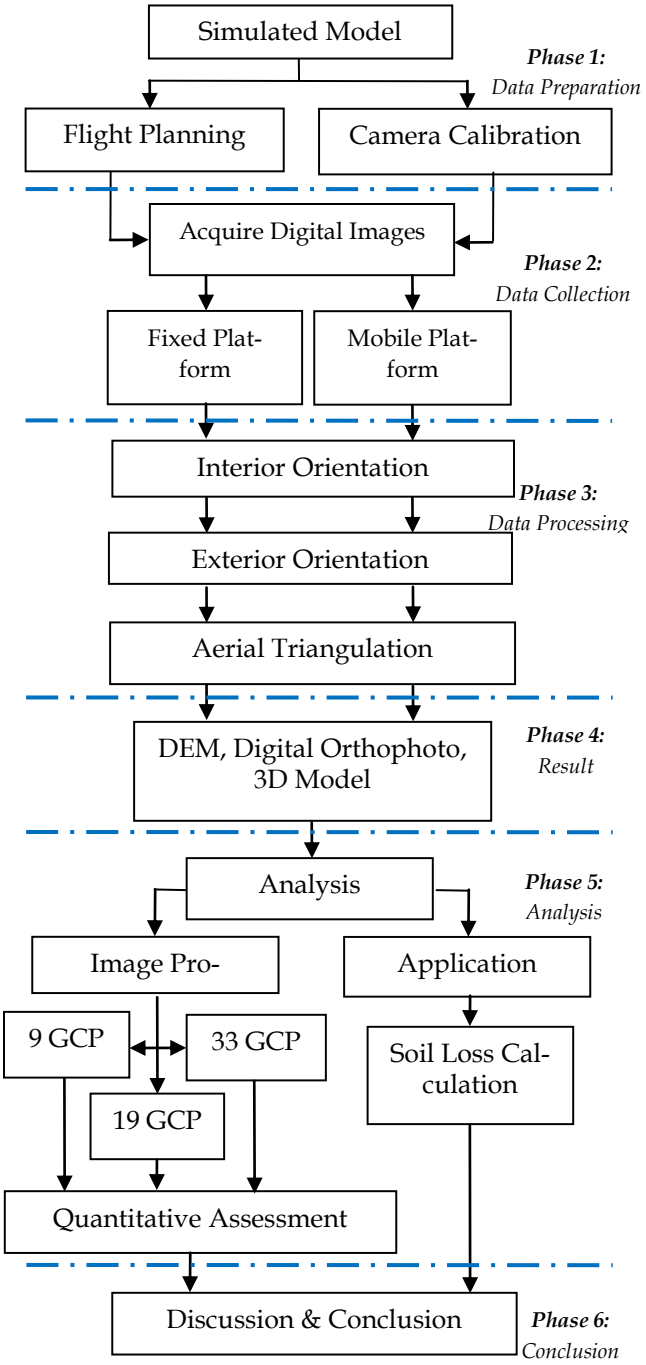

Fig. 2. Flowchart of the Research Methodology

4 Image Processing & Results

All acquired images were processed using a photogrammetric software known as Erdas Imagine software. This software requires camera information such as pixel size, focal length, radial lens distortion and tangential distortion to carry out interior orientation. All GCPs were registered during exterior orientation. Erdas Imagine software requires a minimum of six tie points or three control points for each pair of overlapped photograph. The difference between fixed platform and mobile platform is the method of image acquisition. Fixed platform is built by using a stable platform while mobile platform uses a UAV to capture images. Results of the fixed platform should be more stable and accurate as compare to the mobile platform. The distribution of GCPs and tie points are illustrated in the footprint of Figure 3 and 4 for fixed platform and mobile UAV platform respectively.

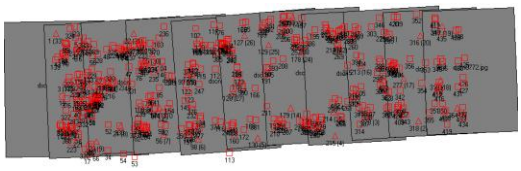

Fig. 3. Footprint for 11 photographs of the GCPs and tie points (fixed platform)

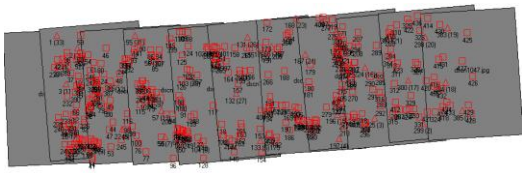

Fig. 4. Footprint for 11 photograph of the GCPs and tie points (mobile platform)

33 GCPs and 11 check points were established using a total station evenly in the simulated model. The coordinates of the GCPs were used as an accepted value or 'true value' for the purpose of accuracy assessment determination. However, 33 GCPs and 404 tie points were established during image processing for fixed platform while 33 GCPs and 353 tie points were established during image processing for mobile platform. Two photogrammetric results were generated after performing interior orientation, exterior orientation and aerial triangulation; DEM and digital orthophoto. The generated digital orthophoto for the simulated model using fixed platform and mobile platform are shown in Figure 5 and 6 respectively.

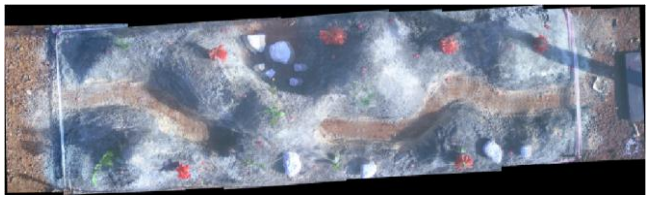

Fig. 5. Digital Orthophoto (fixed platform)

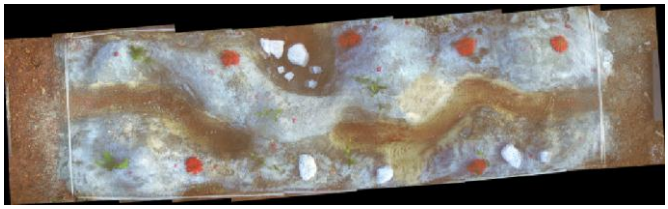

Fig. 6. Digital Orthophoto (mobile platform)

Digital orthophotos for both platforms were compared and were found to be exactly the same except for the color which was caused by a different time exposure and temperature during image acquisition. The resulting orthophotos were the same because the residual error for both platforms was too small. The quality of DEM and digital orthophoto depends on the accuracy of GCPs. Therefore, if the quality of GCP is good, the result of DEM and digital orthophoto should also be accurate. The DEM for both, fixed and mobile platforms are shown in Figure 7 where the visualization of both DEMs are almost similar. In contrast, the result of DEM was found to be less accurate as compared to the orthophoto. One of the factors that affected the accuracy was the affect of motions yaw, pitch and roll during image acquisition. Configuration of GCP also plays an important role in determining the DEM result.

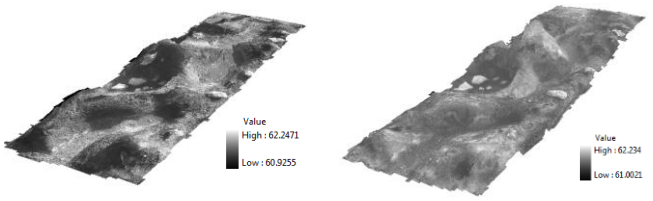

(a) (b)

Fig. 7. DEM: (a) Fixed Platform; (b) Mobile Platform

5 Analysis & Discussion

This study utilized a UAV system for large scale mapping. The first objective of this study is to investigate the use of light weight rotary-wing UAV for mapping a simulated model. The second objective of this study is to determine the accuracy of the photogrammetric output produced from digital image processing. It was found that the UAV system was suitable for large scale mapping with the condition that it was operated by a professional operator during data acquisition. A professional operator is needed in data acquisition in order to control the UAV during flight and to maintain the right path according to the flight planning calculation. The accuracy assessment of DEM and digital orthophotos were evaluated using root mean square error method. In the analysis section, two case studies were investigated using different number of GCP's in aerial triangulation. All acquired images from the fixed and mobile platforms were performed using two different numbers of GCP during aerial triangulation i.e. 33 GCPs, 19 GCPs and 9 GCPs. Results of fixed platform and mobile platform are illustrated in Appendix A and Appendix B respectively. The accuracy of the assessment of DEM and digital orthophoto was based on RMSE, mean, standard deviation and variance of sample data set after image processing. Residual errors for both platforms were also examined to analyze the accuracy of the photogrammetric products. An equation to calculate the errors in photogrammetric product is shown in equation 2.

$$\epsilon = yi - \mu \quad (2)$$

where,

yi = Estimated value
μ = Ground Truth value
ϵ = Error

Appendix A and B shows a sample data of checkpoint for photogrammetric product such as orthophoto and digital elevation model. These results are illustrated more detail in Figure 8. Table 2 and 3 shows statistical results of fixed and mobile platform respectively.

TABLE 2
Statistical Result of Fixed platform

AT	GCP	RMSE (m)	Mean (m)	Std Dev (m)	Variance (m)
33 GCP	X	0.002	0.002	0.002	2.47E-06
404 TP	Y	0.001	0.001	0.001	4.18E-07
	Z	0.214	0.148	0.163	0.0264893
19 GCP	X	0.002	0.002	0.002	2.45E-06
404 TP	Y	0.002	0.002	0.001	8.73E-07
	Z	0.215	0.147	0.165	0.027201
9 GCP	X	0.004	0.003	0.003	9E-06
404 TP	Y	0.002	0.002	0.001	1.364E-06
	Z	0.207	0.158	0.140	0.019548

AT: Aerial Triangulation; GCP: Ground Control Points; TP: Tie Points

TABLE 3
Statistical Result of Mobile platform

AT	GCP	RMSE (m)	Mean (m)	Std Dev (m)	Variance (m)
33 GCP	X	0.002	0.002	0.002	2.45E-06
353 TP	Y	0.002	0.001	0.001	6.18E-07
	Z	0.223	0.156	0.167	0.027956
19 GCP	X	0.002	0.002	0.002	3.02E-06
353 TP	Y	0.002	0.001	0.001	1.47E-06
	Z	0.221	0.150	0.170	0.028835
9 GCP	X	0.003	0.002	0.001	1.564E-06
404 TP	Y	0.001	0.001	0.001	7.636E-07
	Z	0.182	0.146	0.113	0.0126625

AT: Aerial Triangulation; GCP: Ground Control Points; TP: Tie Points

Table 2 and 3 describe the effect of different number of GCP's and tie points during image processing. These criteria are significant to determine the accuracy of the photogrammetry product using different number of GCP's and tie points during image processing. Figure 8 shows the residual mean square error chart for this study. It was found that residual errors increases with lesser number of ground control points, with an exception for the Z-axis data for mobile platform, in which the errors increase with more control points.

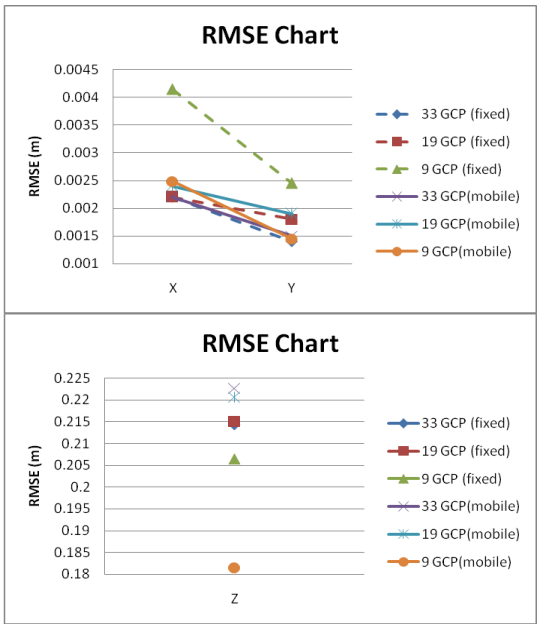

Fig. 8. RMSE Chart (a) RMSE x,y ; (b) RMSE z

Figure 8(a) conclude that the results of RMSE for x and y coordinate changes when the number of control points are changed. Figure 8(b) concludes that the mean square errors between both platforms changes when the number of GCPs used in image processing is different. Number of GCPs and tie points play an important role in image processing. This result proves that the accuracy of photogrammetric product will increase with more GCPs. The accuracy of data can be analyzed using the linear equation as follows;

$$Y = a + bX \quad (3)$$

Where,

Y = Measured Value
a,b = Coefficient
X = Estimated Value

Appendix C (fixed platform) and Appendix D(mobile platform) describe a pattern of check point error using line 1:1 (red line).Appendix C (a,b,c) shows a graph of comparison between the estimated value (photogrammetric technique) and the measured value (ground truth) for X, Y and Z coordinate respectively. From Appendix C (a)(b) and (c), the error of X and Y coordinate was located along the red line which gave good accuracy while some of the Z coordinates were underestimate and some of them were overestimate based on line 1:1 (red line in graph). It can be concluded that the Z coordinates were less accurate than X and Y coordinate. This graph also shows the effect of the number of GCPs in image processing. None of the Z coordinates were located in the red line when the GCP numbers were reduced to nine. This means that the number of GCPs contribute a significant impact in image processing for photogrammetric product.

Appendix D (a,b,c) shows a graph of comparison between the estimated value (photogrammetric technique) and the measured value (ground truth) for X, Y and Z coordinate respectively. Based on Appendix D (a), (b) and (c), the error of X and Y coordinates were located along the red line 1:1. This indicates that the X and Y coordinates gave accurate photogrammetric results. In contrast, the Z coordinates recorded an underestimate and some overestimate error based on line 1:1 (red line in graph). In general, Z coordinates for 33 GCPs and 19GCPs were found to be much more precise as compared to Z coordinates with only 9 GCPs. Therefore the number of GCPs in image processing influences the accuracy and precision of photogrammetric products. Apendix C and Appendix D also record minimum absolute errors (Min. AE), maximum absolute errors (Max. AE) and mean absolute errors (Mean AE). The equation of mean absolute error is as follows

$$\text{Mean AE} = \frac{1}{n}\sum_{n=1}^{n} |yi - \mu| \quad (4)$$

where,

Mean AE = Mean Absolute Error
n = Number of dataset
yi = Estimated value
μ = Measured Value

The result of volume determination is based on the accuracy of the slope data. Therefore, a second analysis can only be done after the accuracy of slope has been determined. The second analysis of this study involves volume determination of landslide and soil loss. The simulated model was excavated to simulate a landslide incident for large scale mapping. Figure 9 shows the direction of contour lines before landslide occurrence and after, in 3D visualization. As a result, the contour lines followed the direction of the landslide. This landslide is represented by a TIN (Triangulated Irregular Network) model for visualizing the three dimensional model of the simulated landslide. The TIN models were produced using ArcGIS 9.3 software. In general, the soil loss can be calculated by subtracting DEM before landslide and after landslide. Surface volume tools are available in ArcGIS 9.3 to calculate surface volume automatically. As a result the volume of soil loss was calculated by subtracting the two different surface volumes before and after the landslide that was generated from both digital elevation model respectively.

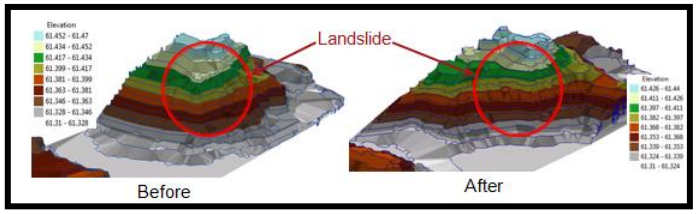

Fig.9. Superimposition between TIN and contour lines before and after landslide

The sum of soil loss of the landslide is 0.002043 meter^3 and the area of landslide is 0.000026 meter^2. In order to prove that this result is close to the actual values, conventional method is used for comparison. The real soil loss is calculated in cylinder cube with a diameter of 23cm and 5cm in height. The volume

calculation in cylinder cube is 2077.38cm³ or 0.002077 meter³. The difference of volume between these two methods is 0.000034 meter³ which is about 1.64% and it is acceptable due to insignificant difference.

6 Conclusion

The objective of this study is to investigate the capabilities of a UAV system in slope mapping using simulated model. This study also compares the UAV data with fixed platform data to analyze the accuracy of the photogrammetric product produced by both methods. It is crucial to carry out a simulated model study before conducting a real site experiment to predict the outcome. In this study, it was found that the light weight rotary-wing UAV was successfully used for capturing the images of the simulated model for small-scale mapping. The digital images were successfully processed to generate DEM. Future study could be carried out using various flying heights and subsequently determine the accuracy. This study also shows that the accuracy of the photogrammetric output from both types of platforms are similar. It is anticipated that the results could change if different flying is used for both platform since this study covers almost the same flying heights and the distance from the simulated model for both the mobile and the fixed platform, in which they were both at low heights and close to the object. Finally, it can be concluded that the UAV could be used for small-scale mapping as demonstrated in this study

Acknowledgment

Faculty of Architecture, Planning and Surveying Universiti Teknologi MARA (UiTM) and Faculty of Geoinformation & Real Estate, Universiti Teknologi Malaysia (UTM) are greatly acknowledged.

References

[1] M. Bryson and S. Sukkarieh, "Architecture for Cooperative Airborne Simulataneous Localization and Mapping," Journal of Intelligent Robot System, vol. 55, pp. 267-297, 2009.

[2] A. Cesetti, E. Frontoni, A. Mancini, A. Ascani, P. Zingaretti, and S. Longhi, "A Visual Global Positioning System for Unmanned Aerial Vehicles Used In Photogrammetric Applications," Journal of Intelligent Robot System, vol. 61, pp. 157-168, 2011.

[3] H.Y. Chao, Y.C. Cao, and Y.Q. Chen, "Autopilots for Small Unmanned Aerial Vehicles: A Survey," International Journal of Control, Automation and Systems, vol. 8, no. 1, pp. 36-44, 2010.

[4] U. Coppa, A. Guarnieri, F. Pirotti, and A. Vettore, "Accuracy Enhancement Of Unmanned Helicopter Positioning With Low-Cost System," Applied Geomatic, vol. 1, pp. 85-95, 2009.

[5] G.J. Grenzdoffer, A. Engel, and B. Teichert, "The Photogrammetric Potential of Low Cost UAVs in Forest and Agriculture," The International Archives of the Photogrammetry, Remote Sensing and Spatial Information Sciences, Vol. XXXVII. Part B1. Beijing, China, 2008.

[6] A. Hervouet, R. Dunford, H. Piegay, B. Belletti, and M.L. Tremelo, "Analysis of Post-Flood Recruitment Patterns In Braided-Channel Rivers At Multiple Scales Based On An Image Series Collected By Unmanned Aerial Vehicles, Ultra-Light Aerial Vehicles And Satellites," Geographical Information Science & Remote Sensing, vol. 48, no. 1, pp. 50-73, 2011.

[7] A. Jaakkola, J. Hyyppa, A. Kukko, X. Yu, H. Kaartinen, M. Lehtomaki, and Y. Lin, "A Low-Cost Multi-Sensoral Mobile Mapping System And Its Feasibility For Tree Measurements," International Society for Photogrammetry and Remote Sensing Journal of Photogrammetry and Remote Sensing, vol. 65, pp. 514-522, 2010.

[8] B. Li, X. Sheng, A. Xia, E. Chengwen, and B. Li, "Actualize of Low Altitude Large Scale Aerophotography and Geodesic base on Fixed-wing Unamanned Aerial Vehicle Platform," The International Archives of the Photogrammetry, Remote Sensing and Spatial Information Sciences, Vol. XXXVII. Part B1. Beijing, China, 2008.

[9] F. Remondiono, and C. Fraser, "Digital Camera Calibration Methods: Considerations and Comparisons," International Society for Photogrammetry and Remote Sensing Commission V Symposium Image Engineering and Vision Metrology. International Archives of Photogrammetry and Remote Sensing, vol. XXXVI, Part 5, pp. 266-272, 2006.

[10] D.G. Schmale III, B.R. Dingus, and C. Reinholtz, "Development and Application of An Autonomous Unmanned Aerial Vehicle For Precise Aerobiological Sampling Above Agricultural Fields," Journal of Field Robotics, vol. 25, no. 3, pp. 133-147, 2008.

[11] K. Schwarz, and N. El-Sheimy, "Mobile Mapping System- State of the Art and the Future Trends Istanbul," International Archives of Photogrammetry and Remote Sensing, vol. XXXV, Part B1, 2004.

[12] D.H. Shim, J.S. Han, and H.T. Yeo, "A Development of Unmanned Helicopters for Industrial Applications," Journal of Intelligent Robot System, vol. 54, pp. 407-421, 2009.

[13] K.N. Tahar and A. Ahmad, "Capability of Low Cost Digital Camera for Production of Orthophoto and Volume Determination," 7th International Colloquium on Signal Processing & Its Applications IEEE, Penang, Malaysia, 2011.

[14] K.N. Tahar, A. Ahmad and W.A.A. Wan Mohd Akib, "Unmanned Aerial Vehicle Technology for Low Cost Landslide Mapping," 11th South East Asian Survey Congress and 13thInternational Surveyor's Congress, Putra World Trade Centre, Kuala Lumpur, Malaysia, 2011.

[15] L. Yan, Z. Gou, and Y. Duan, "A UAV Remote Sensing System: Design and Tests: Geospatial Technology for Earth Observation Data", (eds) Li Deren, Shan Jie, Gong Jianya. New York : Springer-Verlag, 2011.

Appendix A : Residual Error (Fixed Platform)

33 Ground Control Point

Check Points (CP)	Estimated (m)			Ground Truth (m)			Residual (m)		
	X	Y	Z	X	Y	Z	X	Y	Z
CP1	625065.361	174330.854	61.628	625065.360	174330.855	61.464	0.001	-0.001	0.164
CP2	625065.394	174330.831	61.446	625065.389	174330.833	61.532	0.005	-0.002	-0.086
CP3	625065.421	174330.853	61.387	625065.420	174330.854	61.310	0.001	-0.001	0.077
CP4	625065.447	174330.843	62.212	625065.451	174330.845	61.639	-0.004	-0.002	0.573
CP5	625065.528	174330.861	61.260	625065.527	174330.859	61.321	0.001	0.002	-0.061
CP6	625065.468	174330.815	61.000	625065.468	174330.813	61.308	0.000	0.002	-0.308
CP7	625065.349	174330.830	61.237	625065.350	174330.830	61.312	-0.001	0.000	-0.075
CP8	625065.327	174330.807	61.307	625065.326	174330.806	61.353	0.001	0.001	-0.046
CP9	625065.376	174330.802	61.219	625065.376	174330.801	61.383	0.000	0.001	-0.164
CP10	625065.487	174330.810	61.487	625065.488	174330.811	61.427	-0.001	-0.001	0.060
CP11	625065.533	174330.814	61.381	625065.535	174330.815	61.394	-0.002	-0.001	-0.013

19 Ground Control Point

Check Points (CP)	Estimated (m)			Ground Truth (m)			Residual (m)		
	X	Y	Z	X	Y	Z	X	Y	Z
CP1	625065.360	174330.854	61.620	625065.360	174330.855	61.464	0.000	-0.001	0.156
CP2	625065.394	174330.831	61.445	625065.389	174330.833	61.532	0.005	-0.002	-0.087
CP3	625065.422	174330.853	61.392	625065.420	174330.854	61.310	0.002	-0.001	0.082
CP4	625065.447	174330.843	62.218	625065.451	174330.845	61.639	-0.004	-0.002	0.579
CP5	625065.528	174330.863	61.263	625065.527	174330.859	61.321	0.001	0.004	-0.058
CP6	625065.468	174330.815	61.000	625065.468	174330.813	61.308	0.000	0.002	-0.308
CP7	625065.349	174330.829	61.237	625065.350	174330.830	61.312	-0.001	-0.001	-0.075
CP8	625065.328	174330.805	61.381	625065.326	174330.806	61.353	0.002	-0.001	0.028
CP9	625065.377	174330.802	61.224	625065.376	174330.801	61.383	0.001	0.001	-0.159
CP10	625065.487	174330.810	61.497	625065.488	174330.811	61.427	-0.001	-0.001	0.070
CP11	625065.534	174330.814	61.382	625065.535	174330.815	61.394	-0.001	-0.001	-0.012

9 Ground Control Point

Check Points (CP)	Estimated (m)			Ground Truth (m)			Residual (m)		
	X	Y	Z	X	Y	Z	X	Y	Z
CP1	625065.361	174330.854	61.345	625065.360	174330.855	61.464	0.001	-0.001	-0.119
CP2	625065.394	174330.831	61.339	625065.389	174330.833	61.532	0.005	-0.002	-0.193
CP3	625065.421	174330.853	61.435	625065.420	174330.854	61.310	0.001	-0.001	0.125
CP4	625065.451	174330.847	61.752	625065.451	174330.845	61.639	0.000	0.002	0.113
CP5	625065.524	174330.860	61.275	625065.527	174330.859	61.321	-0.003	0.001	-0.046
CP6	625065.467	174330.812	61.107	625065.468	174330.813	61.308	-0.001	-0.001	-0.201
CP7	625065.350	174330.830	61.325	625065.350	174330.830	61.312	0.000	0.000	0.013
CP8	625065.328	174330.806	61.345	625065.326	174330.806	61.353	0.002	0.000	-0.008
CP9	625065.376	174330.801	61.352	625065.376	174330.801	61.383	0.000	0.000	-0.031
CP10	625065.488	174330.812	61.445	625065.488	174330.811	61.427	0.000	0.001	0.018
CP11	625065.538	174330.816	61.467	625065.535	174330.815	61.394	0.003	0.001	0.073

Appendix B: Residual Error (Mobile Platform)

33 Ground Control Point

Check Points (CP)	Estimated (m)			Ground Truth (m)			Residual (m)		
	X	Y	Z	X	Y	Z	X	Y	Z
CP1	625065.361	174330.854	61.626	625065.360	174330.855	61.464	0.001	-0.001	0.162
CP2	625065.394	174330.832	61.444	625065.389	174330.833	61.532	0.005	-0.001	-0.088
CP3	625065.421	174330.852	61.391	625065.420	174330.854	61.310	0.001	-0.002	0.081
CP4	625065.447	174330.844	62.230	625065.451	174330.845	61.639	-0.004	-0.001	0.591
CP5	625065.527	174330.862	61.263	625065.527	174330.859	61.321	0.000	0.003	-0.058
CP6	625065.469	174330.815	60.986	625065.468	174330.813	61.308	0.001	0.002	-0.322
CP7	625065.348	174330.830	61.240	625065.350	174330.830	61.312	-0.002	0.000	-0.072
CP8	625065.327	174330.807	61.434	625065.326	174330.806	61.353	0.001	0.001	0.081
CP9	625065.376	174330.802	61.200	625065.376	174330.801	61.383	0.000	0.001	-0.183
CP10	625065.487	174330.810	61.485	625065.488	174330.811	61.427	-0.001	-0.001	0.058
CP11	625065.533	174330.814	61.379	625065.535	174330.815	61.394	-0.002	-0.001	-0.015

19 Ground Control Point

Check Points (CP)	Estimated (m)			Ground Truth (m)			Residual (m)		
	X	Y	Z	X	Y	Z	X	Y	Z
CP1	625065.360	174330.854	61.620	625065.360	174330.855	61.464	0.000	-0.001	0.156
CP2	625065.394	174330.832	61.424	625065.389	174330.833	61.532	0.005	-0.001	-0.108
CP3	625065.421	174330.853	61.394	625065.420	174330.854	61.310	0.001	-0.001	0.084
CP4	625065.446	174330.844	62.233	625065.451	174330.845	61.639	-0.005	-0.001	0.594
CP5	625065.527	174330.864	61.265	625065.527	174330.859	61.321	0.000	0.005	-0.056
CP6	625065.469	174330.815	60.988	625065.468	174330.813	61.308	0.001	0.002	-0.320
CP7	625065.348	174330.829	61.238	625065.350	174330.830	61.312	-0.002	-0.001	-0.074
CP8	625065.328	174330.805	61.340	625065.326	174330.806	61.353	0.002	-0.001	-0.013
CP9	625065.377	174330.802	61.229	625065.376	174330.801	61.383	0.001	0.001	-0.154
CP10	625065.487	174330.810	61.494	625065.488	174330.811	61.427	-0.001	-0.001	0.067
CP11	625065.534	174330.814	61.370	625065.535	174330.815	61.394	-0.001	-0.001	-0.024

9 Ground Control Point

Check Points (CP)	Estimated (m)			Ground Truth (m)			Residual (m)		
	X	Y	Z	X	Y	Z	X	Y	Z
CP1	625065.361	174330.853	61.491	625065.360	174330.855	61.464	0.001	-0.002	0.027
CP2	625065.394	174330.832	61.179	625065.389	174330.833	61.532	0.005	-0.001	-0.353
CP3	625065.422	174330.854	61.215	625065.420	174330.854	61.310	0.002	0.000	-0.095
CP4	625065.447	174330.844	61.275	625065.451	174330.845	61.639	-0.004	-0.001	-0.364
CP5	625065.529	174330.861	61.192	625065.527	174330.859	61.321	0.002	0.002	-0.129
CP6	625065.470	174330.816	61.177	625065.468	174330.813	61.308	0.002	0.003	-0.131
CP7	625065.351	174330.830	61.454	625065.350	174330.830	61.312	0.001	0.000	0.142
CP8	625065.328	174330.807	61.191	625065.326	174330.806	61.353	0.002	0.001	-0.162
CP9	625065.378	174330.802	61.288	625065.376	174330.801	61.383	0.002	0.001	-0.095
CP10	625065.487	174330.812	61.364	625065.488	174330.811	61.427	-0.001	0.001	-0.063
CP11	625065.533	174330.814	61.344	625065.535	174330.815	61.394	-0.002	-0.001	-0.050

Appendix C: Fixed Platform (a) 33 GCPs ; (b) 19 GCPs ; (c) 9 GCPs

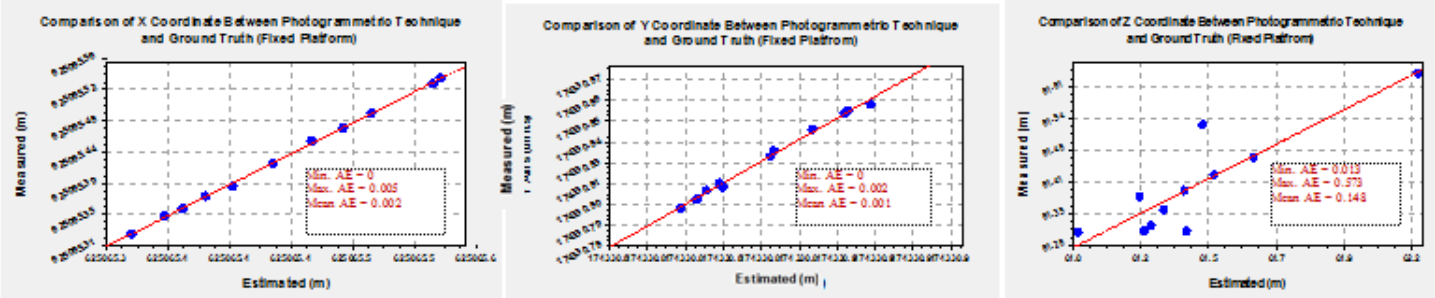

(a)

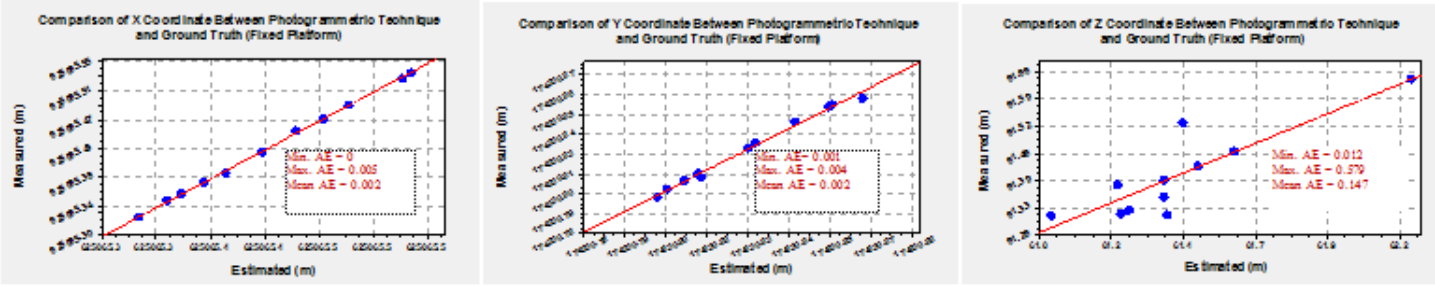

(b)

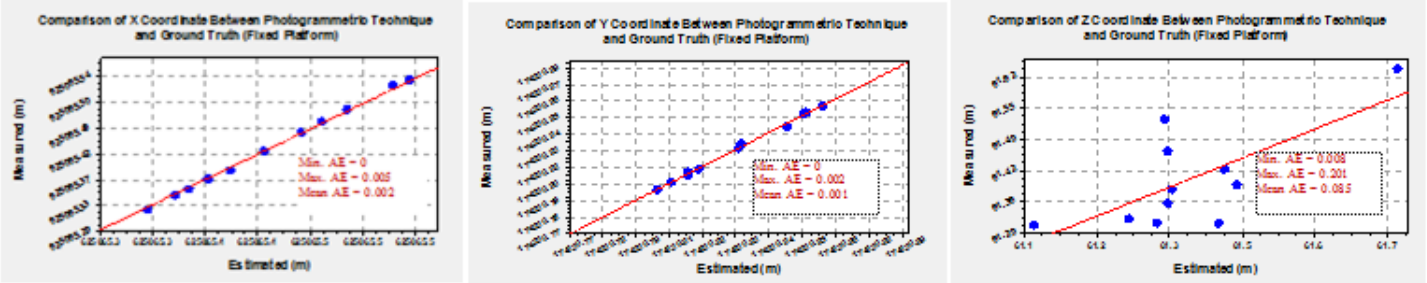

(c)

Appendix D: Mobile Platform (a) 33 GCPs ; (b) 19 GCPs ; (c) 9 GCPs

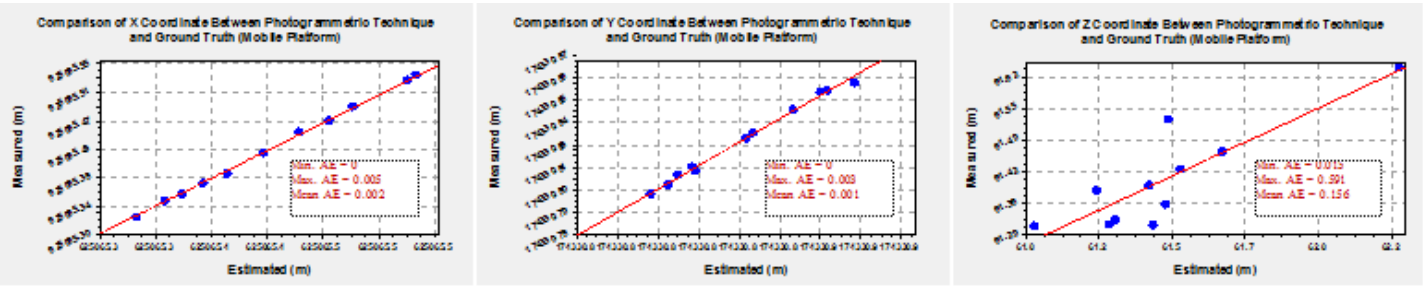

(a)

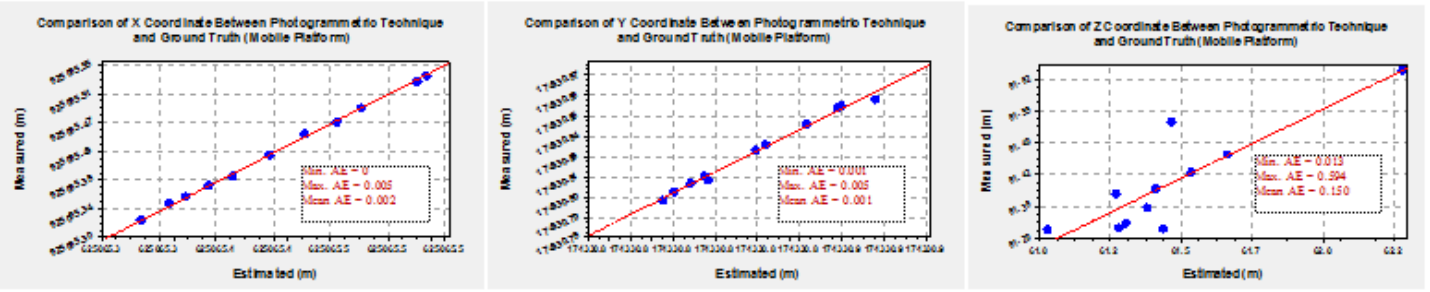

(b)

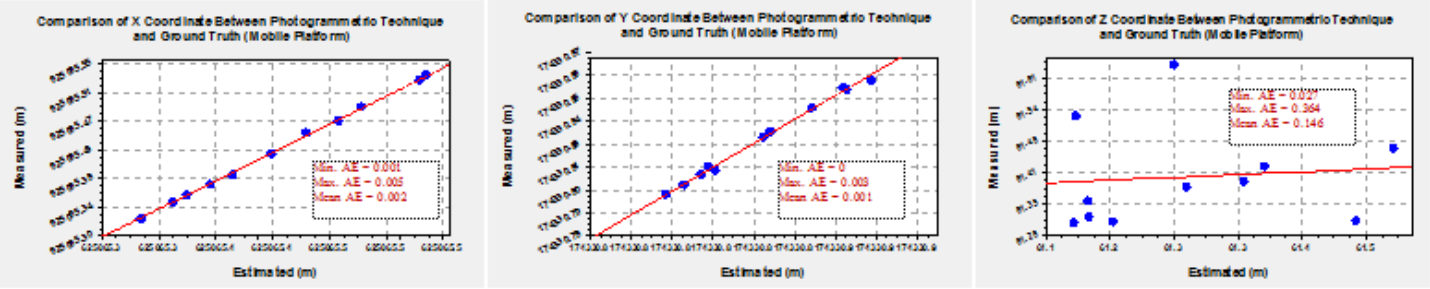

(c)